MULTI-WAVELENGTH STUDY OF GALACTIC REGIONS WITH

HIGH SPECTRAL INDICES IN SUB-mm

Wanchalerm Khwammai

A Thesis Submitted in Partial Fulfillment of the Requirements for the

Degree of Master of Science in Physics

Suranaree University of Technology

Academic Year 2017

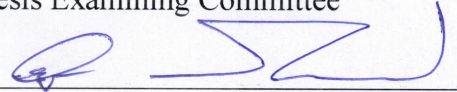# การศึกษาบริเวณกาแลกซีทางช้างเผือกที่มีค่าดัชนีสเปกตรัมสูงด้วยรังสีหลายช่วงความยาวคลื่น
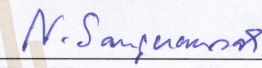
วันเฉลิม ความใหม่

MULTI-WAVELENGTH STUDY OF GALACTIC REGIONS

WITH HIGH SPECTRAL INDICES IN SUB-mm

Suranaree University of Technology has approved this thesis submitted in partial fulfillment of the requirements for a Master's Degree
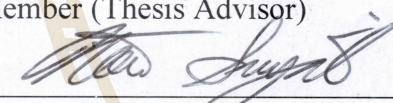
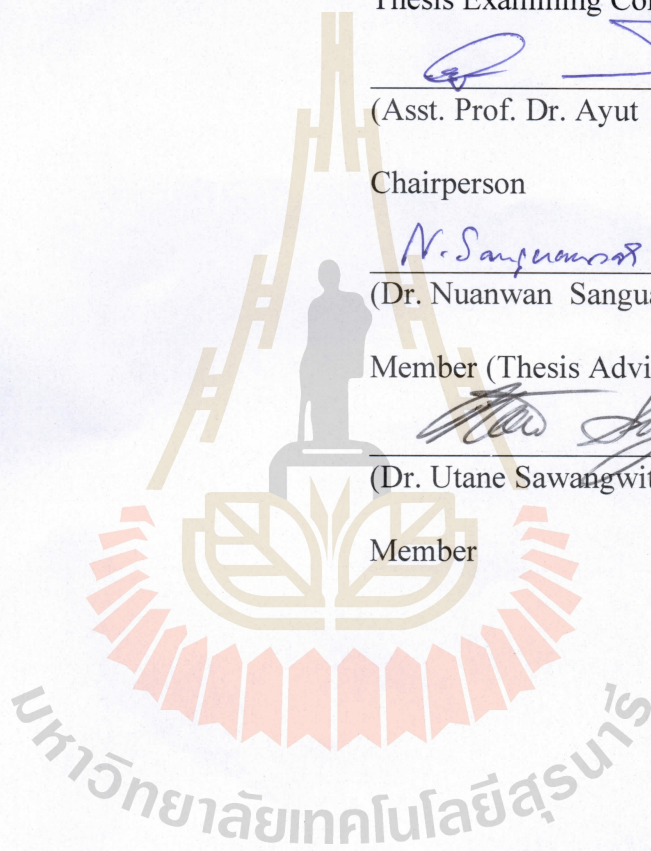Thesis Examining Committee

_____

(Asst. Prof. Dr. Ayut Limphirat)
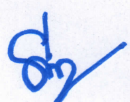
Chairperson

_____

(Dr. Nuanwan Sanguansak)

Member (Thesis Advisor)

_____
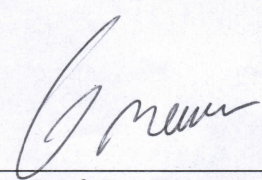
(Dr. Utane Sawangwit)

Member

_____   _____

(Prof. Dr. Santi Maensiri)   (Assoc. Prof. Dr. Worawat Meevasana)

Vice Reactor for Academic Affairs   Dean of Institute of Science

and Internationalization
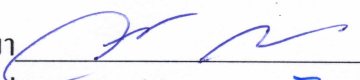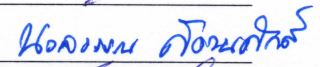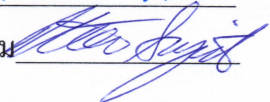
วันเฉลิม ความใหม่ : การศึกษาบริเวณกาแลกซีทางช้างเผือกที่มีค่าดัชนีสเปกตรัมสูงด้วย
รังสีหลายช่วงความยาวคลื่น (MULTI-WAVELENGHT STUDY OF GALACTIC
REGIONS WITH HIGH SPECTRAL INDEX IN SUB-mm) อาจารย์ที่ปรึกษา :
อาจารย์ ดร.นวลวรรณ สงวนศักดิ์, 40 หน้า.

วิทยานิพนธ์นี้ ได้นำเสนอการศึกษาบริเวณใกล้ระนาบกาแลกซีของเรา ที่มีค่าดัชนี
สเปกตรัมประมาณ 9 จากการคำนวณค่าดัชนีสเปกตรัม โดยใช้ข้อมูลอุณหภูมิในช่วงความถี่ 143 217
และ 353 กิกะเฮิรตซ์ จากดาวเทียมแพลงค์ ปกติแล้วดัชนีสเปกตรัมจะมีค่าประมาณ 3-4 ซึ่งเป็นผลที่
เกิดจากการปลดปล่อยพลังงานของแก๊สร้อน และยากที่จะทำการสังเกตการณ์ด้วยย่านวิทยุความถี่
สูงได้ ดังนั้นจึงเป็นที่น่าสนใจที่จะศึกษาบริเวณเหล่านี้อย่างละเอียดโดยใช้ข้อมูลหลายช่วงความยาว
คลื่น (อินฟราเรด อัลตราไวโอเลต เอกซ์เรย์ และ แกมมาเรย์) เพื่อศึกษาปรากฏการณ์ที่เป็นไปได้ที่
ทำให้เกิดค่าดัชนีสเปกตรัมสูงนี้ จากผลการศึกษาพบว่าในย่านความยาวคลื่นอินฟราเรด และ
อัลตราไวโอเลต แสดงถึงความเป็นไปได้ที่ว่าบริเวณดังกล่าวเป็นผลเนื่องมาจากการปลดปล่อย
พลังงานของกลุ่มดาวที่กำลังเกิดใหม่ และถูกกล้อมด้วยคลื่นกระแทกที่เกิดจากซุปเปอร์โนวา

สาขาวิชาฟิสิกส์
ปีการศึกษา 2560

ลายมือชื่อนักศึกษา _____
ลายมือชื่ออาจารย์ที่ปรึกษา _____
ลายมือชื่ออาจารย์ที่ปรึกษาร่วม _____

WANCHALERM KHWAMMAI : MULTI-WAVELENGTH STUDY OF
GALACTIC REGIONS WITH HIGH SPECTRAL INDICES IN SUB-mm.
THESIS ADVISOR : NUANWAN SANGUANSAK, Ph.D. 40 PP.

SPECTRAL INDEX/ MULTI-WAVELENGTH/ GALACTIC STRUCTURE

In this work, we present a study of regions near the Galactic plane with unusually high spectral index around 9, which was calculated using PLANCK temperature maps for frequency bands 143, 217 and 353 GHz. Usually, the radiation from Galactic plane region in these frequency ranges is dominated by thermal dust emission with typical spectral index around 3 to 4. It is rather challenging to study such a large region at this sub-mm frequencies with a high-frequency radio survey. Therefore, the multi-wavelength data, infrared, ultraviolet (FUV and NUV), x-ray and gamma-ray observational data are considered as the indicator for a signpost of the strong astronomical phenomenal. We have found that flux of UV radiation in the unusually high spectral index regions is higher than in the normal spectral index regions, and these locations are represented to the hot young star cluster and supernova remnant.

School of Physics

Academic Year 2017

Student's Signature

Advisor's Signature

Co-advisor's Signature

ACKNOWLEDGMENTS

This thesis could not have been completed without the support of many people.

First, I would like to express my special thank to my advisor Dr.Nuanwan Sanguansak for her supporting, giving me the golden opportunity to have a great experience on astronomy, research in Korea and China, very good comment and teaching me not only research but also life beyond the university since my second year of undergrad.

I am deeply grateful to my co-advisor Dr.Utane Sawangwit from National Asreonomical Research Institute of Thailand (Public Organization) for his advice and teaching me many new things in astrophysics since my bachelor degree.

My thanks also go to all lecturers, staff (especially Khun Phenkhae) and students in the School of Physics, Institute of Science, SUT, for supporting me.

I would also like to thank the Development and Promotion of Science and Technology Talent Project (DPST) for full scholarship since my bachelor's degree.

Lastly and most important, I am most thankful for my parent and everything they have done for me.

Wanchalerm Khwammai

CONTENTS

CONTENTS (Continued)

CONTENTS (Continued)

LIST OF TABLES

LIST OF FIGURES

LIST OF FIGURES (Continued)

LIST OF FIGURES (Continued)

CHAPTER I

INTRODUCTION

1.1   Research background

This work is a continuing study from my bachelor's project: "A STUDY OF CMB FOREGROUND SPECTRAL INDEX USING PLANCK DATA RELEASE II". The sky temperature data from PLANCK mission was used for calculating the spectral index. Spectral indices can be separated due to radiation mechanisms such as synchrotron radiation, free-free emission, thermal dust emission and spinning dust radiation. From our spectral index calculation, there are some interesting regions with unusually high spectral index near the galactic plane. The high frequency waveband from PLANCK data was dominated by thermal dust emission with spectral index around 3-4. Such emission was released from high temperature dust which can be heated up from nearby stars and protostar. But there are some regions which have unusually high spectral index around 9, therefore there is a possibility that these regions might be affected by combinations of various mechanisms. In this work, we focus on multi-wavelength data probing in these regions, it can better distinguish different underlying radiation responsible for the unusually high spectral index. In the Universe, there are many radiation sources (supernova or supernova remnant, thermal radiation from hot gas, AGN and other),

these mechanisms radiate the electromagnetic wave in wide range of frequencies, the signal from each radiation source will dominant in specific wavelength. Thus, we can

study these mechanisms can be studied using the multi-wavelength observation (radio, infrared, and others). At present, there are many data have been released and some are available for public and they can be used for considering the sources of the unusually high spectral indices in these regions.

1.2   The aim of this work

Firstly, the mechanism that cause unusually high spectral indices area should be explained by using multi-wavelength data. Secondly, study the spectral energy distribution (SED) of many different processes which generate foreground emission, would be used for obtaining the Cosmic Microwave Background (CMB) survey.

This thesis is separated in to 5 chapters. Chapter I presents the overview of this work, why we have to study the unusually high spectral index mechanism and the objective of this work. In chapter II, we present the literature survey and review about the multi-wavelength observation of the Universe (infrared, ultraviolet, X-ray and gamma ray) which are very important to study for this work. The review of astronomical mechanism which possibly make the unusually high spectral index effect is also shown in this chapter. In chapter III, the method and all detail of observation data and many conditions which we use in this work, sources of multi-wavelengths data and comparison method are presented. Result and discussion of the interesting points are shown in the chapter IV. In the last chapter, we present summary of this work and what we can continue study in the future.

CHAPTER II

LITERATURE REVIEW

2.1   The spectral index

Planck satellite was launched for measuring the temperature in each position in the sky, to study CMB radiation by measuring flux or intensity at different positions in the sky using various frequencies. In order to convert intensity to temperature, we use the Planck's law

$$I(v, T) = \frac{2hv^3}{c^2} \left(\frac{1}{e^{\frac{hv}{k_B T}} - 1} \right) \qquad (2.1)$$

Where $I(v, T)$ is the spectral radiance, v is a frequency of observation, T is a temperature, c is a speed of light and k_B is Planck 's constants.

To simplify the conversion of equation (2.1), Rayleigh-Jeans approximation is used. The temperature calculated in this way is called "brightness temperature" and is given by

$$T_b = \frac{I_v c^2}{2kv^2} \qquad (2.2)$$

where T_b is brightness temperature at frequency v.

Then we can derive the spectral index(α) depend on brightness temperature and frequency.

$$T_b = constant \cdot (v^{-2}) \tag{2.3}$$

When T_b equal to v^{-2} multiply by constant, we can simplify that brightness temperature depend on the changing of frequency

$$T_b \propto v^{\beta} \tag{2.4}$$

From equation 2.3 to 2.4, we separate the spectral index to two types because the changing frequency in equation 2.3 power by -2, we define alpha and beta spectral index when $\alpha = \beta$ - 2. We use α for calculate the spectral index from slope of the brightness temperature and frequency, we will minus the spectral index value by 2 for converting to alpha spectral index in equation 2.4.

And spectral index will depend on type of radiations which can be obtained from the slope of brightness temperature and frequency.

$$\alpha = \left(\frac{\Delta \log(T_b)}{\Delta \log(v)} \right) - 2 \tag{2.5}$$

The brightness temperature for each type of emission in each frequency bands (Planck Collaboration, 2015) are shown in figure 2.1. We can estimate the spectral index from slope is around 2~3 in thermal dust spectral band (in frequencies range 70 to 353 GHz).

From equation 2.1 to 2.4, these are depended on the intensity in PLANCK 's law. In this work we concern only frequency range 143, 217 and 353 GHz where we found the unusually high spectral index. We assume that the intensity of PLANCK data in these frequencies have been followed the black body radiation and we assume equation 2.1 to 2.2 using Rayleigh Jeans approximation. In this frequency range we can concern foreground effect from thermal dust radiation only because the brightness temperature of thermal dust is dominated in this frequency range.
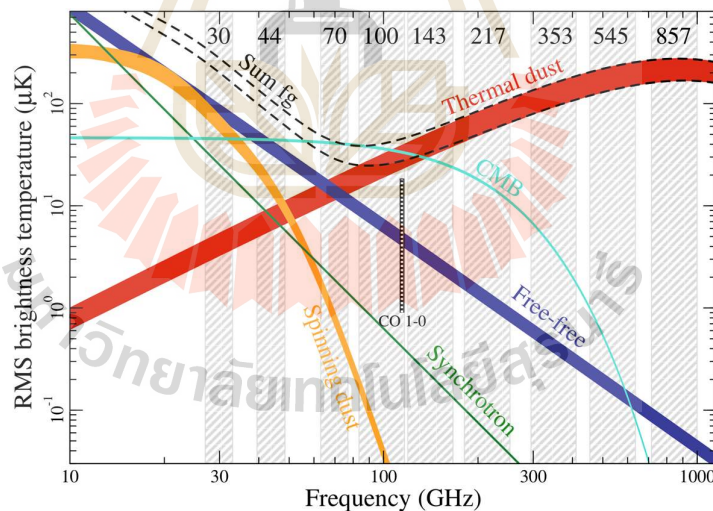
Figure 2.1 Brightness temperature in each type of emission in each frequency bands (Planck Collaboration, 2015).

2.2 Multi-wavelength observation

The multi-wavelength observation is a universe observation in different frequencies band example is radio, X-ray and other. In figure 2.2 shows that the optical observation is a very small range in the all electromagnetic wavelength and can also be transmitted through the Earth's atmosphere. So, the radio and other wavelengths should be used for opening widely to the Universe observation.
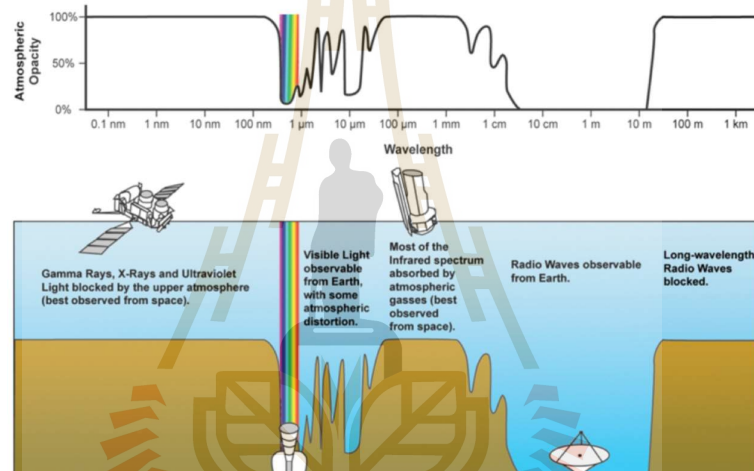
Figure 2.2 Atmospheric electromagnetic transmittance or opacity (*NASA*.gov).

2.3 Radiation sources in the Universe

In the Universe have many objects which can generate electromagnetic radiation, for example the star forming regions, supernova, neutron star, molecular cloud etc., they will release synchrotron radiation, free-free emission, thermal dust emission and other radiation depend on object types. For separating the observation data in order to distinguish type of the radiation, we use multi-wavelength data because

some mechanism will dominate in certain frequency range and cannot be seen in some frequencies.

2.3.1 Molecular cloud observation near the Galactic plane

The unusually high spectral index region locates near the Galactic plane, in this region surrounded by halo of dust and molecular cloud. Therefore, the study the molecular cloud is needed in order to finding the possible mechanism which might cause the unusually high spectral index regions. Hydrogen molecule(H_2) is hardly detected directly therefor we use the evidence of carbon monoxide (CO) because the ratio of CO to H_2 is fairly constants, therefore such gas is concentrated in the spiral arms in discrete "molecular clouds" which are often places of star formation. The CO emission can be observed at 115 GHz (Yuefang T. et al., 2012); (Liu T. et al., 2015). In figure 2.3 shows the molecular cloud observation in some part of the Galactic plane, we can see many of the molecular cloud locate near the galactic plane and maybe surrounding by halo of dust.
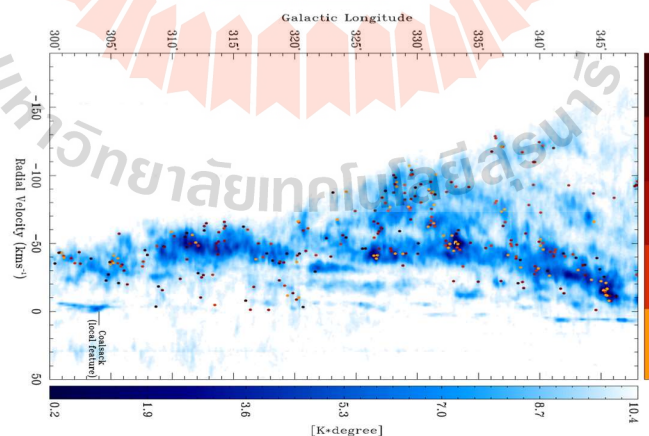
Figure 2.3 The observation of the molecular cloud in some part of the Galactic plane (Bronfman et al., 1996).

2.3.2 Star forming region and hot young star cluster

The star forming region is the area of high-density energy, gravity and temperature. This process released a very strong radiation, probably it has some effect to unusually high spectral index. The star forming region can be found in the high thermal region. Infrared (covered 12, 60, and 100 µm wavelength) and X-ray band (0.25 keV, 0.75 keV, and 1.5 keV) can be used for discovering this region (Kastner et al., 1997); (Clark, 1975)
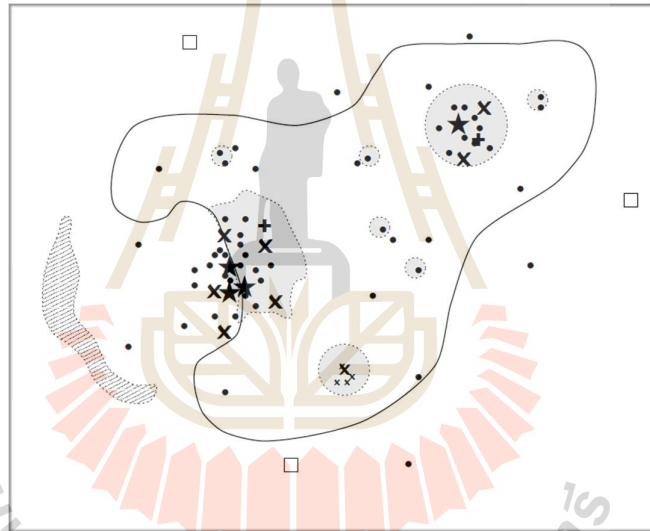
Figure 2.4 Diagram of the expected X-ray components from a giant molecular cloud with a blister HII region, embedded young star clusters and distributed star formation. The hatched region outside of the cloud represents a supernova remnant, and shaded regions within the cloud represent partially ionized X-ray dissociation regions (Feigelson, 2001).

From figure 2.4, the X-ray components observation in giant star formation region have been shown. We can detect wide range of X-ray wavebands from star formation region which depend on type of component (young star, high temperature dust and other mechanism) (Busfield et al., 2006)

The hot young star cluster is one of strong mechanism with release the electromagnetic wave in the universe. Figure 2.5 presents the hot young star cluster emitted the ultraviolet waveband (UV) from its shell and also release line emission from the HII regions and dust which locate inside of this cluster. A few lucky photons can be emitted from the shell of this cluster in UV wave band.
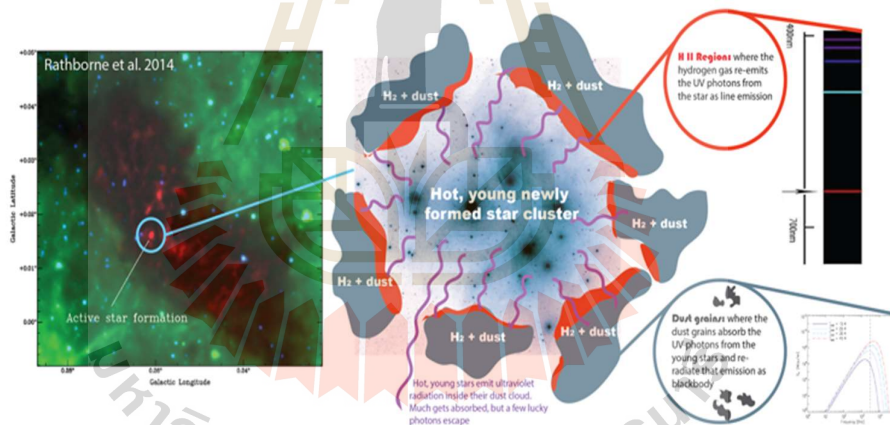
Figure 2.5 The mechanism of UV radiation in the hot young star cluster (Rathborne et al., 2014).

2.3.3   Supernova remnant

Supernova is a very large explosion at the end of stellar evolution. From the large explosion, it spreads very high temperature or energy matter to all direction. As time passes, we can see the evident in form of very high temperature region (normally we call nebula). At the lower energies, the cold interstellar gas strongly absorbs X-rays, and clouds of gas are seen as shadows against background X-ray emission. The different color variations shows the absorption or of the temperatures of the emitting regions. The Galactic plane have the highest-energy X-rays which can pass through the large column densities of gas. The X-rays can use to discovers the supernova remnant (Clark, 1975).

From figure 2.6 shows that the Supernova Remnant (SNRs) can release wide range of infrared wave bands (near-IR, mid-IR and far-IR) (Temim et al., 2012). It depends on the phase of evolution, SNRs in the evolution state released shock wave push the dust to all direction from the Supernova explosion.
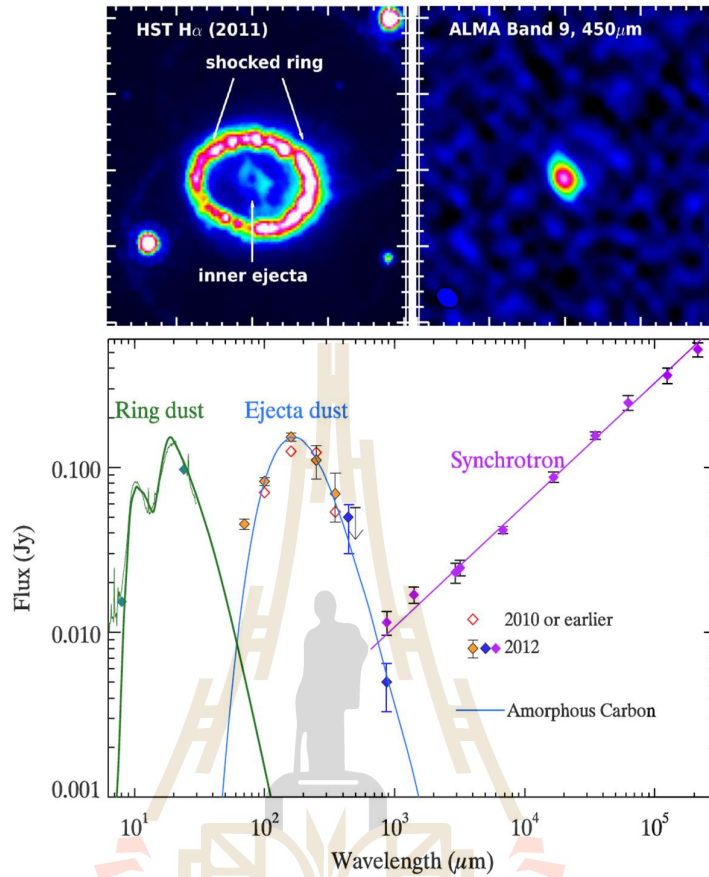
Figure 2.6 Top left: Hubble Space Telescope Ha line image of SN 1987A, showing the equatorial ring and the inner SN ejecta. Top right: ALMA 450 μm continuum image, confirming that the dust emission at far-IR wavelengths spatially coincides with the SN ejecta. Bottom: IR photometric and spectroscopic data for SN 1987A (Temim et al., 2012).

CHAPTER III

METHODOLOGY

3.1 The unusually high spectral index regions

In this work we focused on 2 unusually high spectral index regions from many unusually high spectral index regions which calculated from PLANCK HFI spectral index map. We did not concern other regions because they are located near the strong radiation sources such as Active Galactic Nuclei, the Galactic plane, etc. The center of selected unusually high spectral index regions locate at Galactic latitude and longitude -4.75, -3.16 and 10.63, -19.22 which shown in figure 3.1. Firstly, we obtain the location of the maximum spectral index of each unusually high spectral index regions. Then we set the condition of getting the edge of the unusually high spectral index region where the spectral index decrease to 30% of the maximum spectral index. Finally, we define two axes along North-South (N-S) and east-west (E-W). We found the size is around 127.84 arcmin (E-W) and 106.53 arcmin (N-S) for region 1 and region 2, the size is 64.34 arcmin (E-W) and 72.44 arcmin (N-S). The shape of unusually high spectral index regions are shown in figure 3.2.
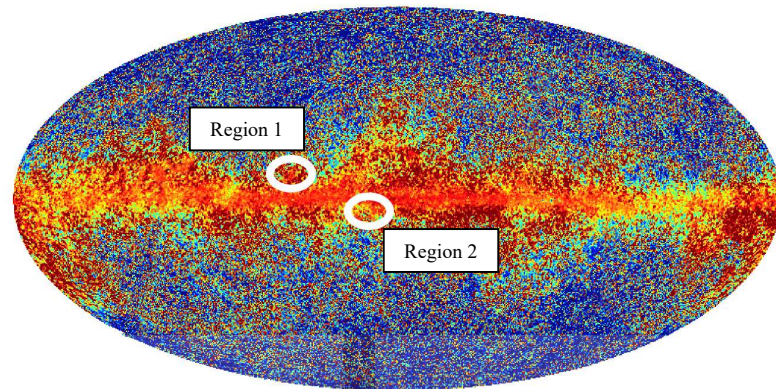
Figure 3.1 The location of the unusually high spectral index regions in white circles.
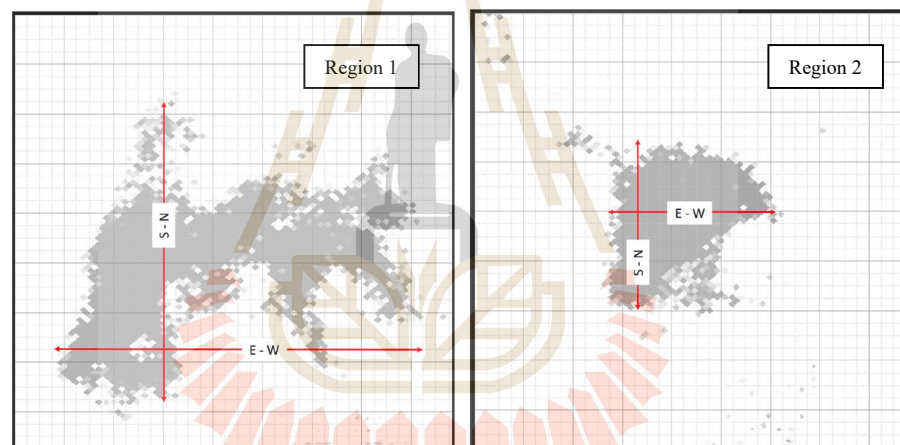
Figure 3.2 The shape of the unusually high spectral index regions.

3.2 Comparing selected regions with the normal regions

In order to compare the unusually high spectral index regions and the normal spectral index regions, we set the condition for the normal spectral index region is the region where the average spectral index is around 3-4. We have selected 10 normal spectral index regions which has the same area size as the unusually high spectral index

regions. The location and detail of these normal spectral index regions are presented in table 3.1.

Table 3.1 The names, locations, map resolution and the map pixel size of each normal spectral index regions.

Name	Location (*l,b*)	Resolution (*arcmin*)	Map size (*arcmin²*)
NR1	23.2284071, 5.63432156	0.3	150x150
NR2	-43.3234491, 5.00930132	0.3	150x150
NR3	-61.5000453, 5.62252000	0.3	150x150
NR4	-60.8769584, -2.53832132	0.3	150x150
NR5	-25.4547002, -2.53491113	0.3	150x150
NR6	-35.6572240, -1.53455660	0.3	150x150
NR7	35.0025604, -1.344091243	0.3	150x150
NR8	35.1907544, 3.29632156	0.3	150x150
NR9	44.5847330, 2.70432305	0.3	150x150
NR10	70.6758343, 2.70945673	0.3	150x150

The spectral index map and temperature map of 10 normal comparison regions are presented in figure 3.3 and the spectral index map and temperature map at 143 GHz of unusually high spectral index regions shown in figure 3.4. The unit of temperature in this work is Kelvin CMB.
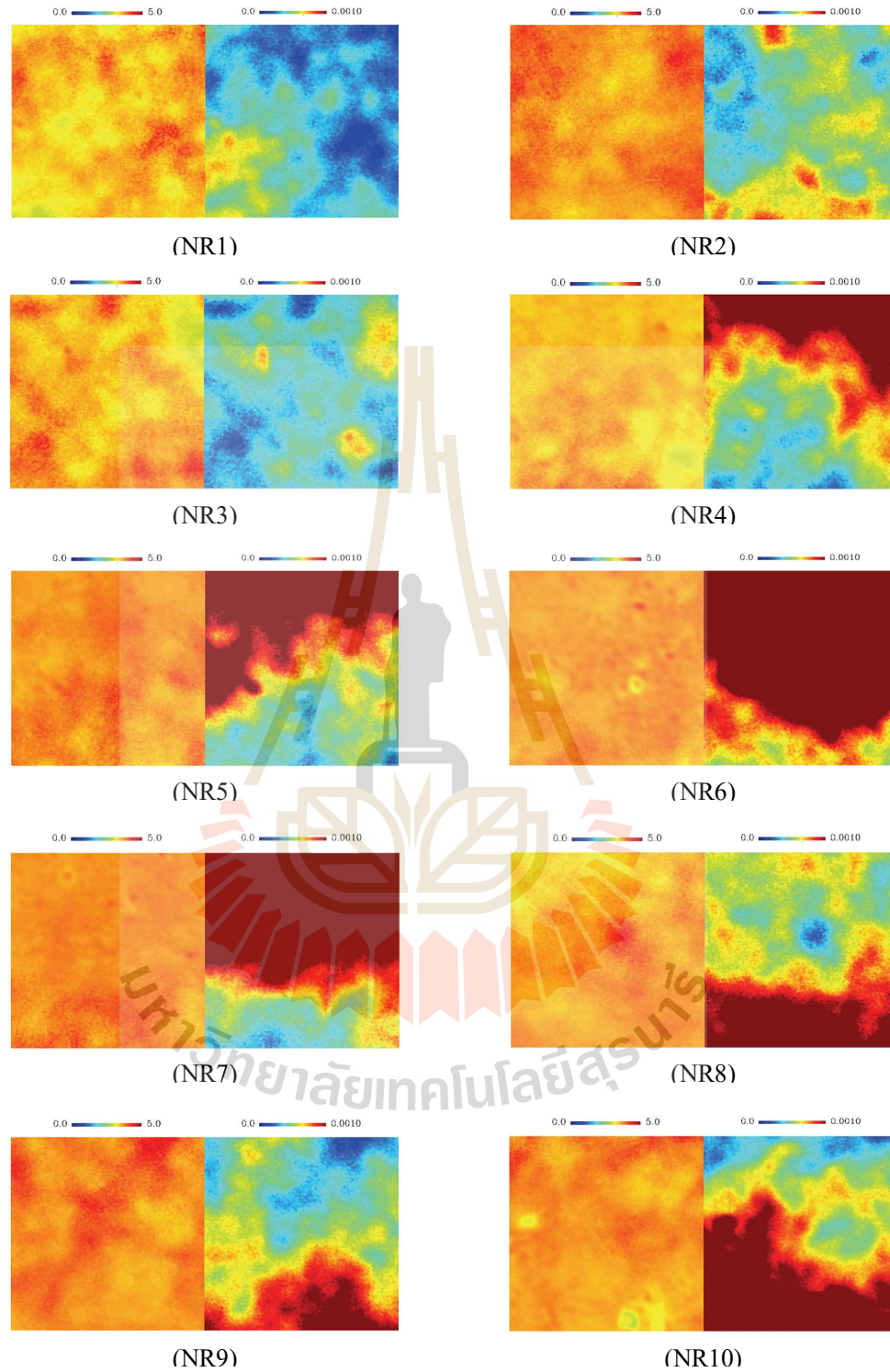
Figure 3.3 The spectral index map (left) and temperature map at 143 GHz (right) of

the normal spectral index region 1 to 10 (NR1-NR10), temperature in unit of K_CMB.

Unusually high spectral index region 1

Unusually high spectral index region 2
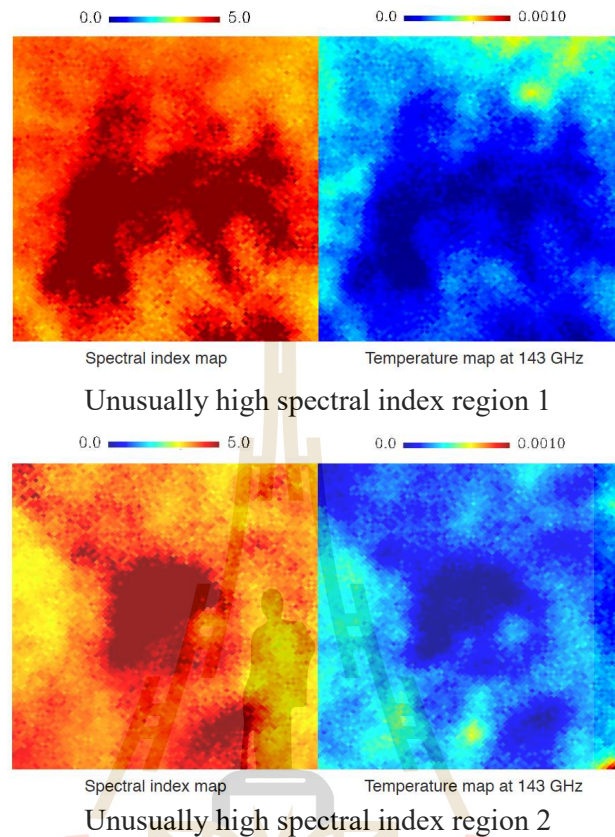
Figure 3.4 The spectral index map (left) and temperature map at 143 GHz (right) of the unusually high spectral index regions, temperature in unit of K_CMB.

3.3   Multi-wavelengths data

In order to cover all frequencies spectrum: infrared, ultraviolet, X-ray and gamma-ray are considered. The result of each waveband will represent some interested astronomical mechanism in the unusually high spectral index region.

3.3.1 Infrared data

We obtained the all sky survey Infrared data from Wide-field Infrared Survey Explorer (*WISE*). *WISE* released first complete all sky survey in infrared data in February 2011, this data is available on *WISE* online public website. The infrared data from *WISE* cover all sky which is shown in figure 3.5.
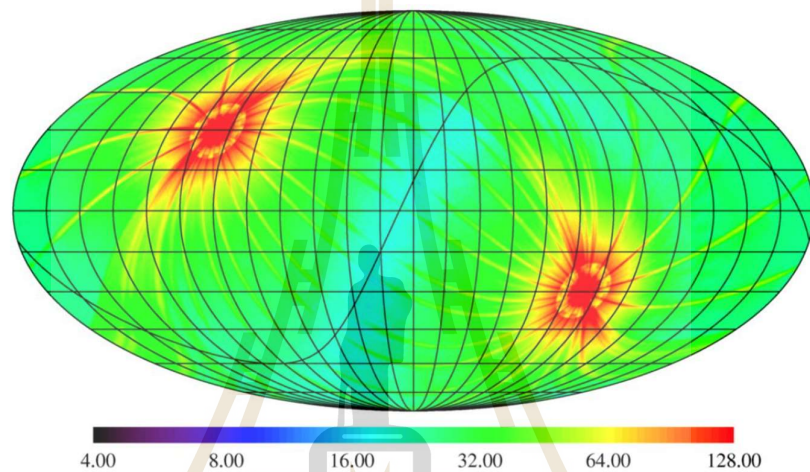
Figure 3.5 *WISE* sky coverage and number of observations in each regions (*WISE*).

3.3.2 Ultraviolet data

We obtained the ultraviolet data from the Galaxy Evolution Explorer (*GALEX*). *GALEX* observe both of Far Ultraviolet (*FUV*) and Near Ultraviolet (*NUV*). *GALEX* did not observe in the region around the Galactic plane and in near the Galactic plane, coverage field on the sky of the *FUV* and *NUV* observation from the *GALEX* are shown in figure 3.6. The UV coverage field condition is an important condition which can be used for selecting the regions for this work (in 3.1 and 3.2).
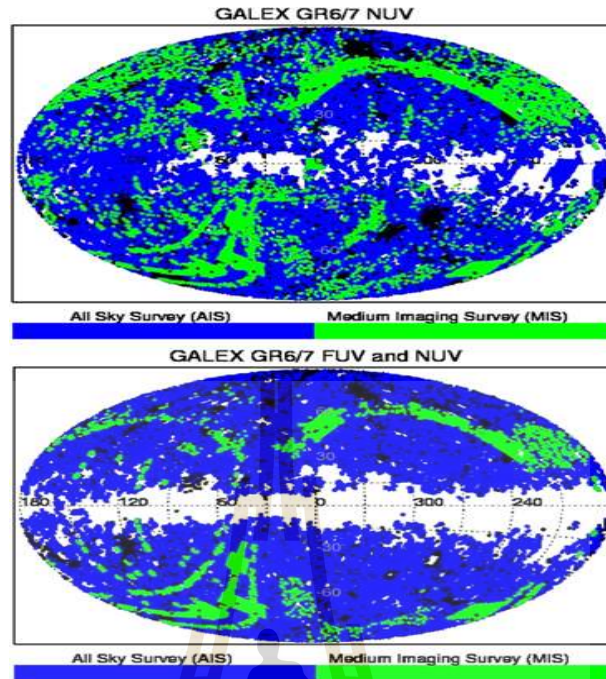
Figure 3.6 *NUV* sky coverage (top) and *FUV* sky coverage (bottom) (Bianchi et al., 2017).

3.3.3   X-ray data

We use the x-ray data from the *ROSAT* X-ray all sky survey. In this wave band we found some problem that the X-ray data not coverage all sky. In the unusually high spectral index region, we do not have full cover area data. Some normal spectral index regions do not have the X-ray data. The X-ray data from *ROSAT* coverage all sky which shown in figure 3.7.

3.3.4   Gamma ray data

In this work we use the gamma ray data which provided by the Fermi mission. The gamma ray data from *Fermi* coverage all sky which shown in figure 3.8. In the same as X-ray data, the data in gamma ray are not covered some regions in the unusually high and normal spectral index regions which we are interested in this work.
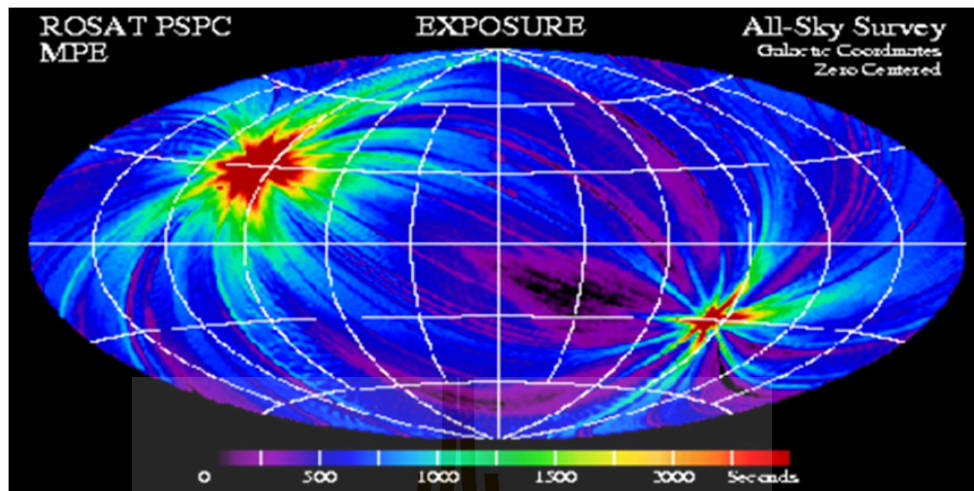
Figure 3.7 Show *ROSAT* sky coverage and exposure time of observation (*NASA*).
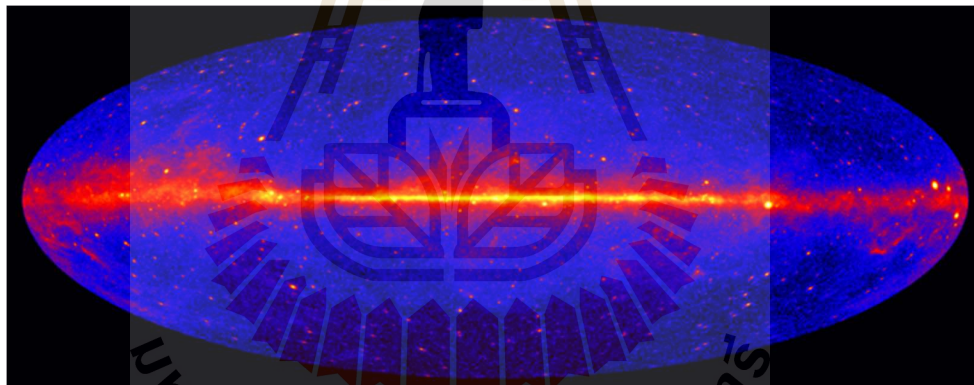
Figure 3.8 Show *Fermi* sky coverage of observation (*NASA*).

3.4 Raw data calibration

One of the most important things in this work is data calibration because we use the multi-wavelengths data from different data sources. We show all detail of raw data in each wavelength in table 3.2. Our aim of this work based on the result which calculated from *Planck* that use for reference calibration. Simplicity of comfortable the

calibration the coordinate of all data needs to change to be the same unit (Galactic coordinate), using IDL. In the IDL we can change the coordinate in fits file (from pixel index to the Galactic coordinate, from Ra/Dec to the Galactic coordinate and other coordinate in fits file to the Galactic coordinate). In this work, we consider unusually high spectral index regions within map size 500 x 500 pixel and angular size or beam width per one pixel from *Planck* is 0.3 *arcmin*. We will use map size and beam width size from *Planck* to reference for calibration.
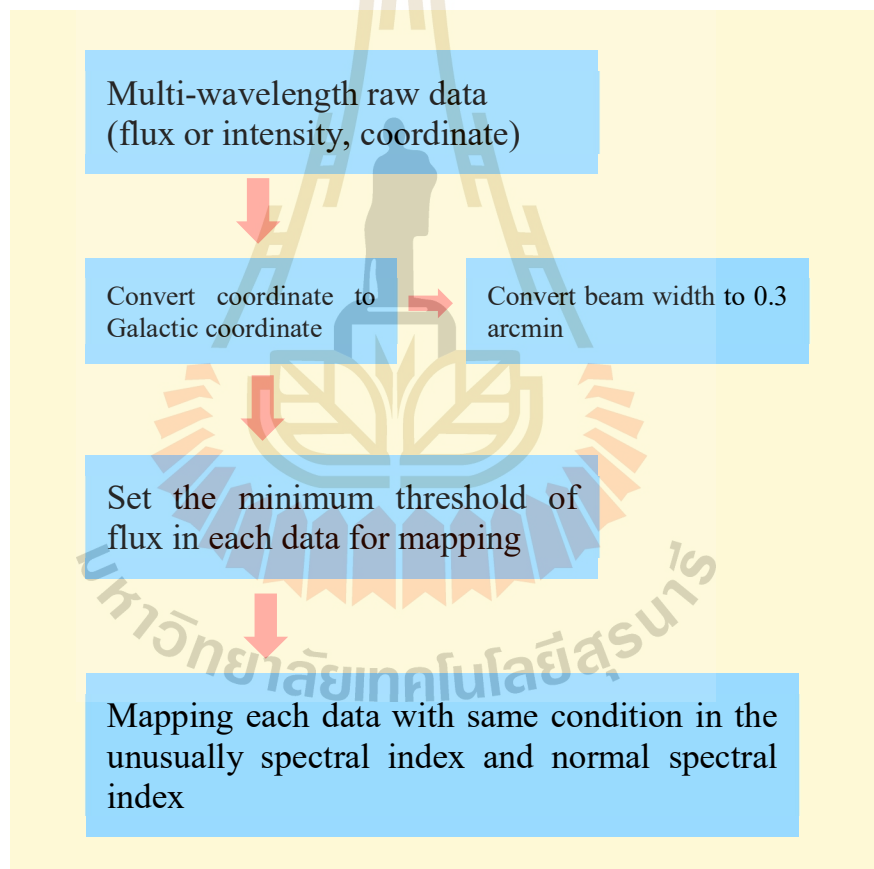
Figure 3.9 Overview of diagram for doing this work.

Table 3.2 The details of data which are used in this work.

Wave bands	Data source	Beam width (*arcmin*)	Sky coverage area (%)	Coordinate	Flux unit
143 GHz	*Planck*	0.30	100%	index of pixel	mJy
Infarred	*WISE*	0.11	100%	Galactic	mJy
Ultraviolet	*GALEX*	0.10	84.4% (*NUV*) 77.3% (*FUV*)	Galactic	magnitude
X-ray	*ROSAT*	0.17	67.3%	*Equatorial*	$cm^{-2}s^{-1}MeV^{-1}sr^{-1}$
Gamma-ray	*Fermi*	0.20	100%	*Equatorial*	$cm^{-2}s^{-1}MeV^{-1}sr^{-1}$

3.5   Histogram and mapping for comparison

We use the histogram for counting number of signals which we consider between the unusually high spectral index regions and the normal spectral index regions, because it clearly shows the different between 2 groups of data. The number of pixels which detected infrared, UV, X-ray and gamma-ray versus logarithm of wavelengths are plotted. For better understanding about mechanism that affected the unusually high spectral index, we plot the location of each signal from multi-wavelength data on to map of the selected regions.

CHAPTER IV

RESULT AND DISCUSSION

4.1 Correlation of location between unusually high spectral index region and low temperature region at frequency 143 GHz

The unusually high spectral index and temperature at frequency 143 GHz are mapped within same location and size 150x150 arcmin. This region has same location as a low temperature region in frequency 143 GHz, shown in figure 4.1. However, in the normal spectral index regions, there is no significant with low temperature at this frequency. The example temperature map of 2 normal spectral index regions as shown in figure 4.1 (B) and (D).

The temperature and spectral index maps indicate that they have a correlation with some low temperature radiation mechanism which is dominated at 143 GHz.

4.2 Multi-wavelength data result

The histogram for counting the number of pixels which can be detected the signal from each waveband (infrared, ultraviolet, X-ray and gamma-ray), in figure 4.2 and 4.3. At the infrared waveband, the number of pixels which detected signals in the unusually high quite equal to number of pixels which deleted signals in the normal spectral index regions (in these plots we average 7 normal regions for consideration,

we cannot use all of 10 comparison regions because some condition about sky coverage- limit of these data).

(A) (B)

(C) (D)
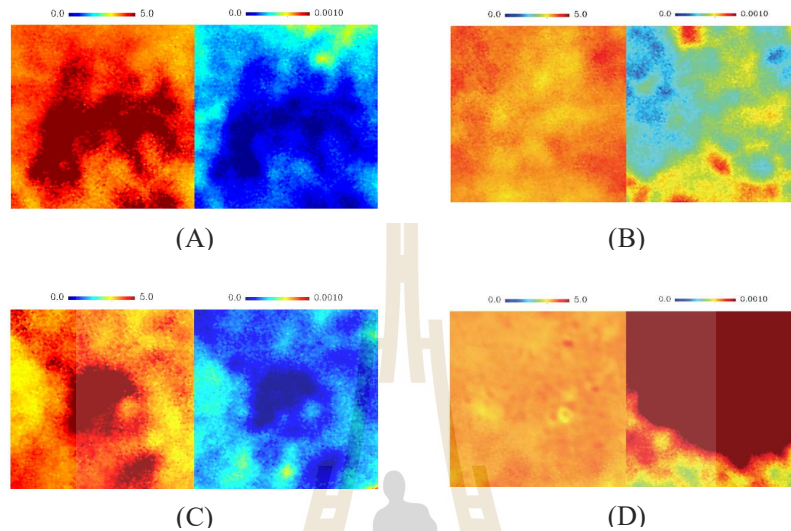
Figure 4.1 The compared maps between spectral index and temperature, (A) spectral index in left side and temperature in right side of unusually high spectral index region 1, (B) spectral index in left side and temperature in right side of normal spectral index region 1, (C) spectral index in left side and temperature in right side of unusually high spectral index region 2, (D) spectral index in left side and temperature in right side of normal spectral index region 7, temperature in unit of K_CMB.

At the *UV* waveband (both of *FUV* and *NUV*), the number of detected pixels in the unusually high higher than in the normal spectral index regions. In the X-ray waveband, the number of signals is very low because the unusually high spectral index regions locate very close to the Galactic plane. The X-ray observation is very difficult to do in these regions because the data was dominated by the radiation from high energetic dust and gas which these surrounded around the Galactic plane. Like the X-ray wave band,

the gamma-ray signals are very low in the unusually high spectral index regions because the observation condition. In the X-ray and gamma-ray wavebands we cannot compare with the normal spectral index regions because the data in these wavebands not coverage in the normal regions.

We project the location of sources for each waveband in to the map of the unusually high spectral index regions.

Figure 4.4 shows the map of the unusually high spectral index region 1, most of UV sources locate in the edge of the region and some of sources locate outside of the region. All of the Infrared data located outside the region. The X-ray and gamma-ray data found one source in this map and locate outside of the region, their presented are not related to the unusually high spectral index.

In figure 4.5 shows the map of the unusually high spectral index region 2, most of UV sources locate in the edge of the region and some of sources locate outside of the region. All of the Infrared data located outside around the region. The X-ray and gamma-ray data found two sources in this map and locate outside of the region, they are not related to unusually high spectral index. The same result is shown in the unusually high spectral index region 1.
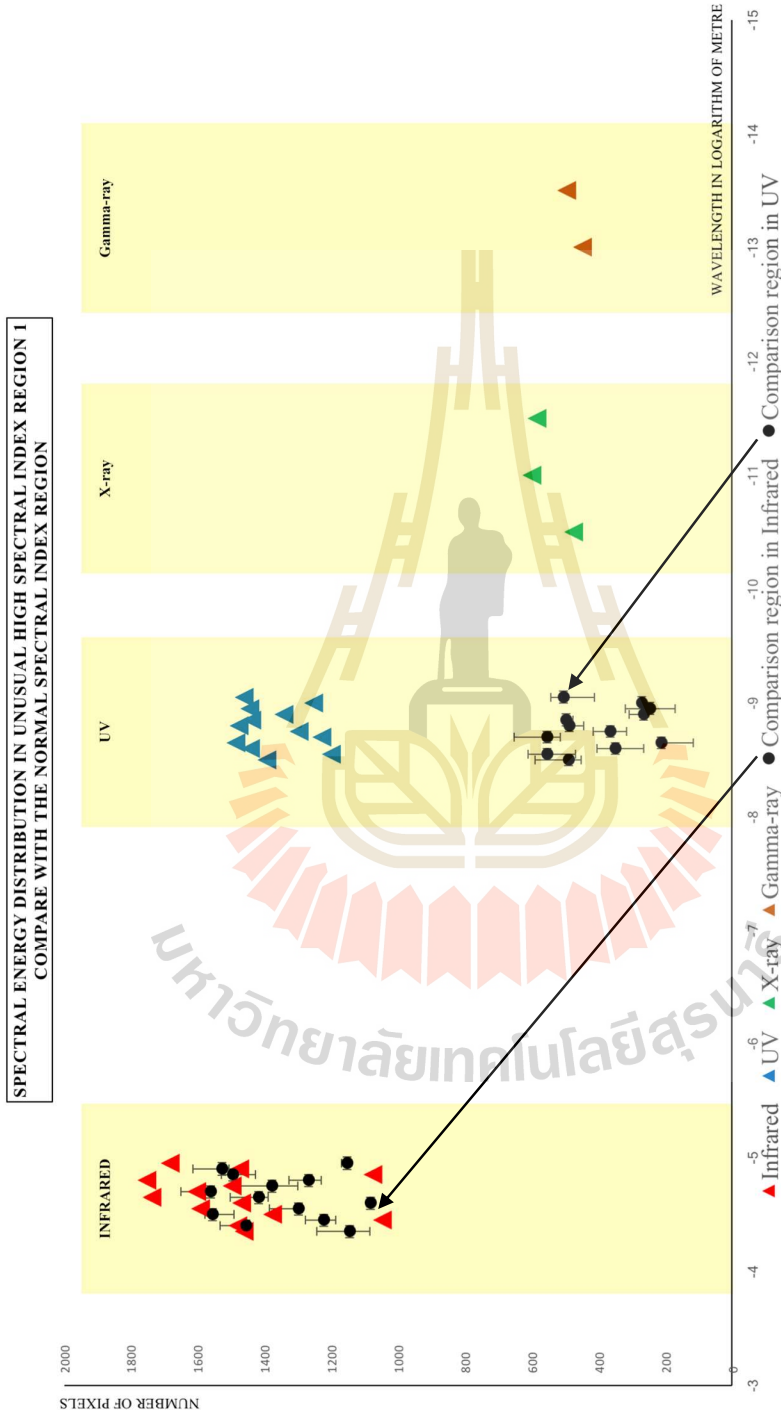
Figure 4.2 Histogram of number of pixels which detected signal in each frequency bands, compare between the observation data in unusually high spectral index region 1 and 7 average the normal spectral index regions.
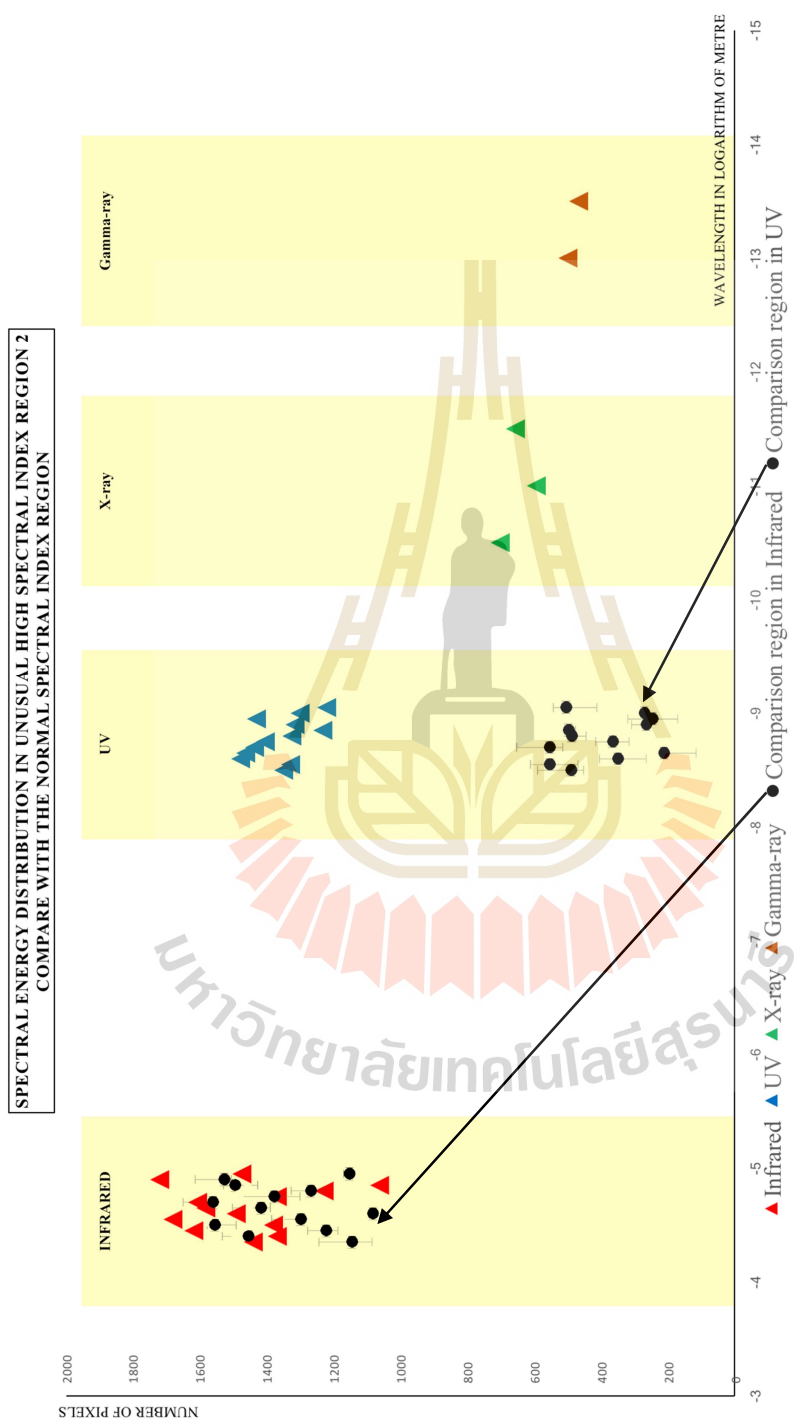
Figure 4.3 Histogram of number of pixels which detected signal in each frequency bands, compare between the observation data in unusually high spectral index region 2 and 7 average the normal spectral index regions.
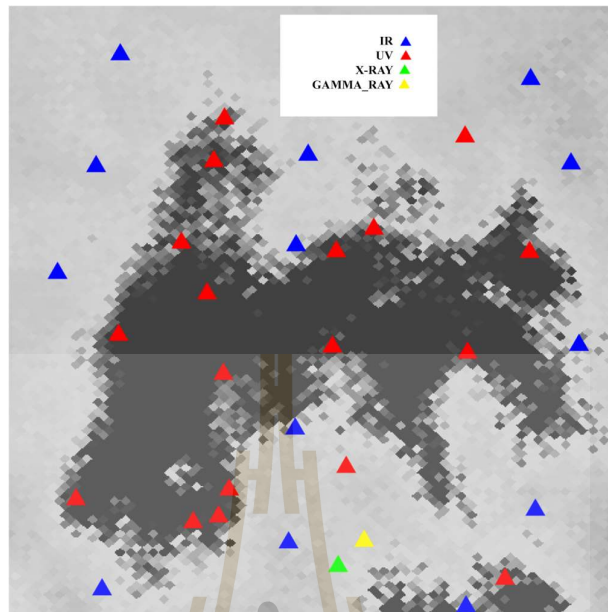
Figure 4.4 Mapping location of center of source in each waveband which detected in the unusually high spectral index region 1.
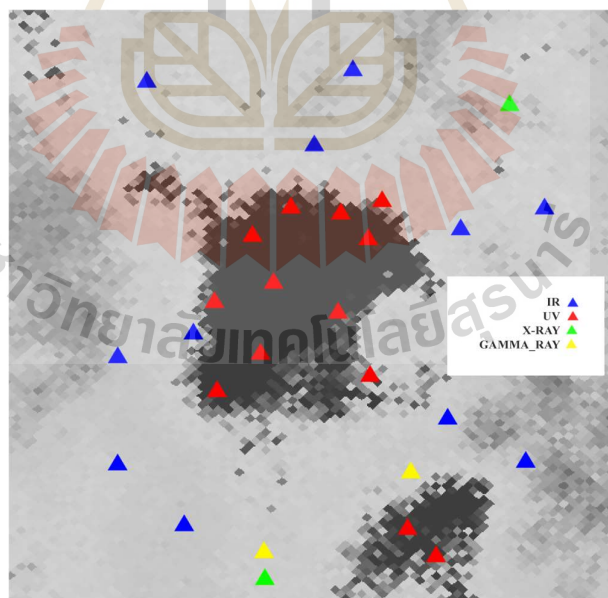
Figure 4.5 Mapping location of center of source in each waveband which detected in the unusually high spectral index region 2.

4.3   The result in the Ultraviolet waveband

From the spectral energy distribution in section 4.2, we found the interesting result in the UV waveband because the signal in the unusually high spectral index regions clearly higher than in the normal spectral index regions. We consider this waveband specifically by adding more detail in the plot this waveband. UV data from GALEX consists of index of pixel location where UV was detected, and we can obtain the flux of UV in each pixel. Then, we plotted the histogram of FUV and NUV for the unusually high spectral index region and the normal spectral index region as shown in figure 4.6 and 4.7. From these figures, we can see that the histogram of pixel numbers which represents FUV and NUV signal within wide range of UV flux (0-100 mJy), both of histograms show similar result. The flux of FUV and NUV in the unusually high spectral index region is higher than the normal spectral index region.
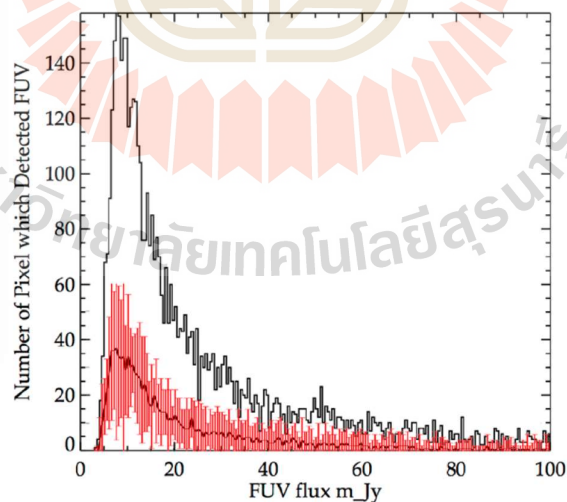
Figure 4.6 Histogram of detected FUV signal pixels in the unusually high spectral index region (top line) and average histogram of detected FUV signal pixels in 7 normal regions (bottom line).
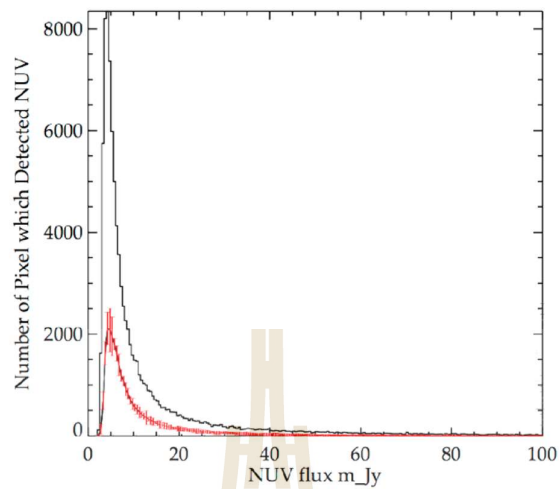
Figure 4.7 Histogram of detected NUV signal pixels in the unusually high spectral index region (top line) and average histogram of detected NUV signal pixels in 7 normal regions (bottom line).

The result in UV shows that the unusually high spectral index regions have some significant with the UV signal, we plot distribution of UV signal in the unusually high spectral index regions in figure 4.8,4.9. From plot of UV distribution, all the UV signal locate in the unusually high spectral index regions.

Figure 4.8 and 4.9, distribution plot shows the clump of FUV and NUV in the unusually high spectral index regions 1 and 2. The threshold for plot the distribution is around 30% from maximum of flux of UV (both of FUV and NUV). In the region1 the clump of FUV quite found more than NUV (around 27%). In the region 2 the clump of FUV quite found more than NUV (around 54%). The ratio of FUV and NUV can represent to the age of the star cluster in these regions. We can predict that the hot star cluster which affect high spectral index is quite young.
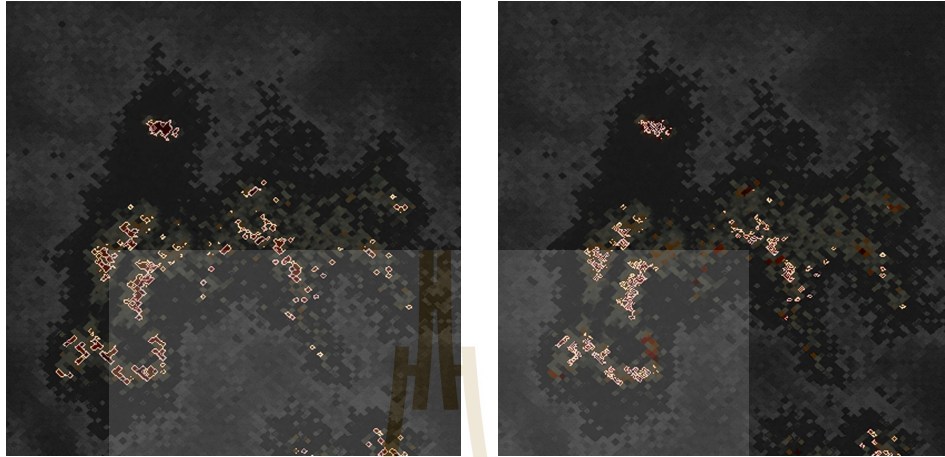
Figure 4.8 Distribution plot of FUV (left) and NUV (right) in the unusually high

spectral index region1 (mapping on to the high spectral index within grey scale).

Figure 4.9 Distribution plot of FUV (left) and NUV (right) in the unusually high

spectral index region2 (mapping on to the high spectral index within grey scale).

CHAPTER V

SUMMARY AND FUTURE WORK

5.1 The relation between unusually high spectral index with low temperature regions at frequency 143 GHz

The unusually high spectral index regions have the same location as the low temperature regions at frequency 143 GHz, it indicates that how the mechanism of unusually high spectral index relates to some unknown low temperature regions. The spectral index, α, directly depends on the difference in the fluxes/temperatures at different frequencies used in the calculation. In this case the difference value is higher because of low temperature at frequency 143 GHz. The low temperature region at 143 GHz indicate that these regions may be surrounded by cold gas which is the essential component of the molecular clouds and star formation regions.

5.2 Summary of multi-wavelengths data

From the result in chapter IV where we used multi-wavelength data for considering the possibility of which mechanism is responsible for the unusually high spectral index regions. The data in infrared, ultraviolet, X-ray and gamma-ray wavebands were studied. The comparisons between the unusually high and normal spectral index regions in these

wavebands show that the mechanism must be dominated by the IR and UV radiation processes.

5.2.1 The shock fronts of Supernova Remnant surrounds the unusually high spectral index region

A Supernova Remnant (SNRs), during its evolution state released shock fronts that push the dust in all direction, from the Supernova explosion happened some time ago. This mechanism expects to emit x-ray radiations via Bremsstrahlung process caused by the shock fronts. Thus, X-ray data were studied in our high spectral index regions. These are taken from ROSAT public data archive. However, we found no evidence of significant X-ray radiation in these regions, as shown in figure 4.4 and 4.5

5.2.2 The hot young star cluster in the unusually high spectral index region

The hot young star cluster emitted both FUV and NUV. From the distribution of the UV emission which mainly located at the edge of regions. This indicates that these regions could be related to the hot young star cluster. We do not observe much UV emission inside of the regions because the hot young star cluster is unusually surround by dust which absorb UV photons and re-emit in IR. However, some UV radiation can still escape from non-uniform lumpy dust shell which partially cover the hot star cluster.

5.3 The expectation model of this region

From all result we draw one of possible model for the unusually high spectral index regions in figure 5.1.
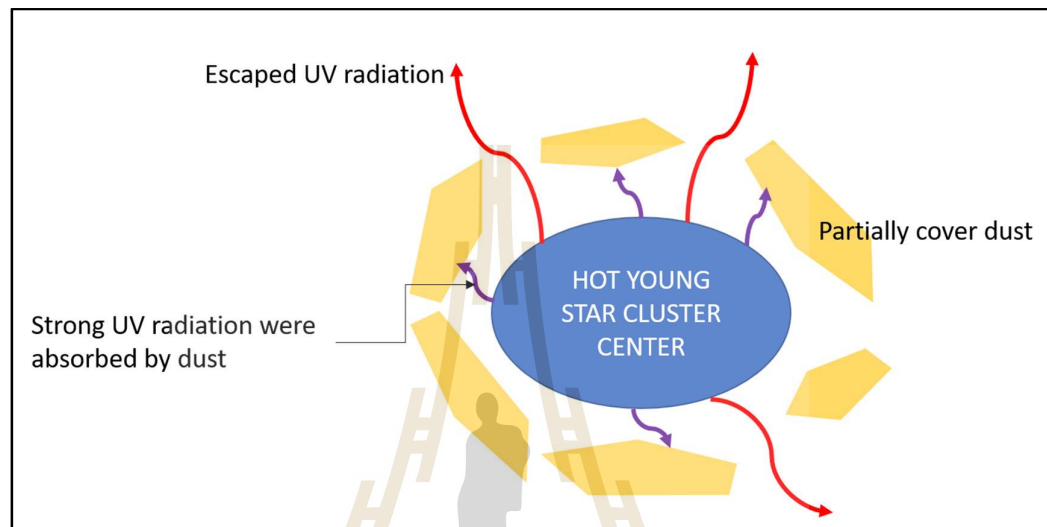
Figure 5.1 Possible model to describe the unusually high spectral index region.

5.4 Future work

From the significant of UV in the unusually high spectral index regions and the relation between the hot young star cluster, in the future we could calculate star formation rate in this region from escaped UV flux and attempt to develop a method to directly calculate star formation rate based on the spectral index in sub-mm radio and Far IR wavebands. Moreover, we can study the optical depth from the hot young star cluster model.

The spectral index is easy to calculate from the brightness temperature or flux from various observations. In the future, the spectral index distribution could also be used to model foreground subtraction from the Cosmic Microwave Background data

which are plagued by strong foreground emission from our Galaxy. CMB observation is very important evidence to study the begin of our Universe, it will be highly advantage if we can use the spectral index to increase the quality of primordial CMB data.

REFERENCES

REFERENCES

Adam, R., Aghanim, N., Alves, M. I. R., Aniano, G., Arnaud, M., Ashdown, M. I. R., Aumont, J., Baccigalupi, C., Banday, A. J., Barreiro, R. B., Bartlett, J. G., Battaner, E., Benabed, K., Bersanelli, M., Bielewicz, P., Bobin, J., Bock, J. J., Bonaldi, A., Bond, J. R., Borrill, J., Bouchet, F. R., Boulanger, F., Bridges, M., Bucher, M., Burigana, C., Butler, R. C., Catalano, A., Chamballu, A., Chiang, H. C., Christensen, P. R., Church, S., Clemens, M., Clements, D. L., Colombi, S., Colombo, L. P. L., Combet, C., Couchot, F., Coulais, A., Crill, B. P., Curto, A., Cuttaia, F., Danese, L., Davies, R. D., Davis, R. J., Bernadis, P. D., Rosa, A. D., Zotti, G. D., Delabrouille, J., Dickinson, C., Diego, J. M., Dole, J. M., Donzelli, S., Douspis, M., Draine, B. T., Dupac, X., Efstathiou, G., Eriksen, H. K., Falgarone, E., Finelli, F., Forni, O., Frailis, M., Fraisse, A., Franceschi, E., Galeotta, S., Ganga, K., Ghosh, T., Giard, M., Giardino, G., Gratton, S., Gregorio, A., Grenier, I. A., Gruppuso, A., Guillet, V., Hansen, Hanson, D., Harrison, D. L., Helou, G., Herranz, D., Hildebrandt, S. R., Hivon, E., Hobson, M., Holmes, W. A., Hornstrup, A., Hovest, W., Jewell, J., Joncas, G., Jones, W. C., Juvela, M., Keskitalo, R., Kisner, T. S., Knoche, J., Knox, L., Kunz, M., Lagache, G., Lasenby, A., Laureijs, R. J., Lawence, C. R., Leonardi, R., Lesgourgues, R., Levrier, F., Liguori, M., Lilje, P. B., Lubin, P. M., Maino, D., Mandolesi, N., and Maris, M. (2014). Planck Collaboration: Diffuse component separation: Foreground maps. **A&A** 1502: 1588.

Adam, P. R., Ade, N., Aghanim, M. I. R., Alves, M., Arnaud, M., Ashdown, J., Aumon, C., Baccigalupi, a Gregorio, a Gruppuso, J. E., Gudmundsson, F. K., Hansen, and Hanson, D. (2015). Planck Collaboration: The Planck mission. **A&A** 1502: 01582.

Adam, P. R., Ade, N., Aghanim, M. I. R., Alves, M., Arnaud, M., Ashdown, J., Aumon, C., Baccigalupi, Banday, a J., Bielewicz, P., Bouchet, F. R., a Gregorio, a Gruppuso, J. E., Gudmundsson, F. K., Hansen, and Hanson, D. (2015). Planck Collaboration: Diffuse component separation: CMB maps. **A&A** 1502: 02114.

Bertout, C., Combes, F., Ferrara, A., Forveille, T., Shore, S. N., Tolstoy, E., and Walmsley, C. (2011). Early results from the Planck mission. **A&A** 536: 16.

Bianchi, L., Conti, A., and Shiao, B. (2014). The ultraviolet sky: An overview from the GALEX surveys. **ASR** 53: 900.

Bronfman, L., Nyman, L. A., and May, J. (1996). High mass star forming cloud. **A&A** 115: 81.

Busfield, A. L., Purcell, C. R., and Hoare, M. G. (2006). Infrared study of the southern Galactic star-forming region associated with IRAS 14416-5937. **MNRAS** 366: 1096.

Clark, D. H. (1975). A study of galactic supernova remnant, based on molonglo parker observation data. **Mon Not** 267: 305.

Dupac, X., and Tauber, J. (2005). Scanning strategy for mapping the CMB anisotropies with PLANCK. **A&A** 430: 363.

Feigelson, E. D. (2001), Supernova remnant and Giant cloud clumps. **ASP Conf** 234 : 231.

Indebetouw, R., Matsuura, M., Dwek, E., Zanardo, G., Barlow, M. J., and Baes, M. (2014). Dust Production and Particle Acceleration in Supernova 1987A Revealed with ALMA. **ApJ** 782.

Liu, T., Zhang, Q., Kim, K. T., Wu, Y., Lee, C. W., Lee, J. E., Tatematsu, K., Choi, M., Juvela, M., Thompson, M., Goldsmith, P. F., Liu, S. Y., Naomi, H., Koch, P., Henkel, C., Sanhueza, P., He, J. H., Rivera-Ingraham, A., Wang, K., Cunningham, M. R., Tang, Y. W., Lai, S. P., Yuan, J., Li, D., Fuller, G., Kang, M., Luong, Q. N., Liu, H. B., Ristorcelli, I., Yang, J., Xu, Y., Harota, T., Mardones, D., Qin, S. L., Chen, H. R., Kwon, W., Meng, F., Zhang, H., Kim, M. R., and Yi, H. W. (2015). Planck cold clumps in the orions complex: i. discovery of an extremely youngclass 0 protrostellar object and a proto-brown dwarf candidate in a bright rimmed clump PGCC G192.32-11.88. **A&A** 1511: 09121.

Matsuura, M., Dwek, E., Barlow, M. J., Babler, B., Baes, M., and Meixner, M. (2015). A Stubbornly Large Mass of Cold Dust in the Ejecta of Supernova 1987A. **ApJ** 800: 50.

Temim, T., Slane, P., Arendt, R. G., and Dwek, E. (2012). Infrared and X-Ray Spectroscopy of the Kes 75 Supernova Remnant Shell: Characterizing the Dust and Gas Properties. **ApJ** 745: 46.

Wu, Y., Liu, T., Meng, F., Li, D., Qin, S. L., and Ju, B. G. (2012). Gas emission in PLANCK cold clumps — A survey of the $J = 1$-0 transition of ^{12}CO, ^{13}CO and $C^{18}O$. **ApJ** 756: 76.

CURRICULUM VITAE

NAME   Mr. Wanchalerm Khwammai

DATE OF BIRTH   December 05, 1993

PLACE OF BIRTH   Bangkok, Thailand

PERSONAL ADDRESS   272 Klongsongnham Rd., Tambon Pharuyai

Mueang Nakhon Ratchasima district,

Nakhon Ratchasima, Thailand 30000

CONTACT   Mobile phone : +6694-514-6496

E-mail   : KWM.WCM@gmail.com

EDUCATIONS

M.Sc. (2016 - present)

School of Physics, Suranaree University of Technology, Nakhon

Ratchasima, Thailand

Bachelor of Science (2013 - 2016)

School of Physics, Suranaree University of Technology, Nakhon

Ratchasima, Thailand